ACS APPLIED MATERIALS & INTERFACES

Energy, Environmental, and Catalysis Applications

Tailoring Copper Foam with Silver Dendrite Catalysts for Highly Selective Carbon Dioxide Conversion into Carbon Monoxide

Félix Urbain, PengYi Tang, Nina M. Carretero, Teresa Andreu, Jordi Arbiol, and Joan R Morante

ACS Appl. Mater. Interfaces, **Just Accepted Manuscript** • DOI: 10.1021/acsami.8b15379 • Publication Date (Web): 27 Nov 2018

ACS Publications

is published by the American Chemical Society. 1155 Sixteenth Street N.W., Washington, DC 20036

Tailoring Copper Foam with Silver Dendrite Catalysts for Highly Selective Carbon Dioxide Conversion into Carbon Monoxide

Félix Urbain[1], Pengyi Tang[1,2], Nina M. Carretero[1], Teresa Andreu[1,3], Jordi Arbiol[2,4], and Joan Ramon Morante[1,5]*

[1] IREC, Catalonia Institute for Energy Research, Jardins de les Dones de Negre 1, 08930 Sant Adrià de Besòs, Barcelona, Catalonia, Spain

[2] Catalan Institute of Nanoscience and Nanotechnology (ICN2), CSIC and BIST, Campus UAB, Bellaterra, 08193 Barcelona, Catalonia, Spain

[3] Universitat Politècnica de Catalunya, Jordi Girona 1–3, 08034 Barcelona, Catalonia, Spain

[4] ICREA, Pg. Lluís Companys 23, 08010 Barcelona, Catalonia, Spain

[5] Universitat de Barcelona, Martí i Franquès, 1, 08028 Barcelona, Catalonia, Spain

[*]**Corresponding Author**: E-Mail: furbain@irec.cat

Abstract

The present study outlines the important steps to bring electrochemical conversion of carbon dioxide (CO_2) closer to commercial viability by using a large-scale metallic foam electrode as highly conductive catalyst scaffold. Due to its versatility, it was possible to specifically tailor three-dimensional copper foam through coating with silver dendrite catalysts by electrodeposition. The requirements of high yield CO_2 conversion to carbon monoxide (CO) were met by tuning the deposition parameters towards a homogeneous coverage of the copper foam with nanosized dendrites, which additionally featured crystallographic surface orientations favoring CO production. The presented results evidence that Ag dendrites, owing a high density of planes with stepped (220) surface sites, paired with the superior active surface area of the copper foam can significantly foster the CO productivity. In a continuous flow-cell reactor set-up, CO faradaic efficiencies reaching from 85 % to 96 % for a wide range of low applied cathode potentials (< 1.0 V_{RHE}) along with high CO current densities up to 27 mA/cm^2 were achieved, far outperforming other tested scaffold materials. Overall, this research provides new strategic guidelines for the fabrication of efficient and versatile cathodes for CO_2 conversion compatible with large-scale integrated prototype devices.

KEYWORDS: CO_2 reduction, electrocatalysis, CO production, silver dendrites, copper foam, prototype reactor

1. Introduction

Re-utilization of carbon dioxide (CO_2) is deemed as one of the key challenges to lower the atmospheric CO_2 levels and steer towards a more sustainable future. In this regard, the electrochemical CO_2 reduction reaction (CO_2RR) comes to the fore as an alluring way to convert CO_2 into fuels, chemical and materials. Simultaneously, such an electrochemical process can furthermore allow using on demand excess energy from renewable energy plants.[1] However, to make this technology available at industry level, i.e. to bridge the gap between academic innovation and commercialization, versatile and cost-effective processes at large-scale are still in dire need. In addition to that, highly selective and efficient electroreduction of CO_2 into value-added products is a crucial requirement. The numerous CO_2RR products range from two electron products, such as carbon monoxide (CO) and formic acid (HCOOH),[2-5] to multi-electron products such as methane (CH_4),[6] methanol (CH_3OH),[7] ethylene (C_2H_4),[8] and ethanol (CH_3CH_2OH),[9] as well as other compounds.[10] Due to the complex reaction pathways of CO_2RR, high yield selective product generation remains challenging, and, so far, has only been achieved for CO and formic acid in aqueous solutions. CO is of particular interest, as it can be efficiently separated from other reaction products (separation of liquid products is much more energy-intensive) and because together with hydrogen (H_2) it can be valorized to synthesis gas. From this versatile gas mixture, liquid transportation hydrocarbon fuels and various other value-added chemical products can be produced *via* the well-known and established Fischer-Tropsch synthesis.[11]
As reported to date, high yield and selective production of CO from CO_2 relies on the utilization of precious metal catalysts, typically gold (Au),[12-14] or requires the usage of ionic liquids,[15-17] which however impair the process stability. Investigating systems and processes enabling inexpensive, selective and stable CO_2RR is therefore a crucial requirement for making this process economically viable, as it will be presented in this work. Furthermore, in contrast to the previous laboratory-scale systems, which only demonstrate small-scale sub-assemblies performing CO_2RR, we outline the important steps towards a functional and scalable process to selectively produce CO at large scale and high yield in neutral pH aqueous solution.

In particular, we propose a CO_2RR cathode based on commercial and large-scale metallic foam, which was specifically adapted to meet the stringent requirements for selective CO_2-to-CO conversion. Due to their three-dimensional (3D) structure, metallic foams offer the advantage of high surface area, which is necessary to circumvent the solubility limitations of CO_2 gas in liquid electrolytes and thus enabling efficient CO_2RR catalysis. In this regard, it is important to guarantee a high number of three-phase interfaces, i.e. interfaces where CO_2 gas–liquid electrolyte–solid electrode coincide. The tailoring of the 3D foam consisted firstly in the homogenous coating with optimized silver (Ag) catalysts and secondly, in the optimization of the morphological and structural characteristics of the deposited catalyst. Ag is an attractive alternative to electrodes made of Au for CO_2RR as it exhibits similar selectivity towards CO under moderate overpotentials and is significantly cheaper than most other noble metals.[18,19] Furthermore, nano- or microstructured Ag catalysts can lower even more the required overpotentials[3] while increasing at the same time the density of highly active sites for CO_2RR. In this regard, dendritic structures are of particular interest and were targeted in this study. Besides numerous examples of Ag based materials for CO_2RR to CO, such as nanoplates,[20] nanoporous material and nanoparticles,[21-25] nanowires,[26,27] nanoclusters[28] and porous foams,[29], dendritic structures offer large active surface areas paired with facile and non-expensive synthetization.[30-32] In this regard, we selected the

electrodeposition method to deposit the Ag catalyst. On account of its functionality and cost effectiveness, this deposition process is highly viable for large-scale industrial applications, e.g. the coating of large-scale metallic foams, and therefore promising to fulfil the requirements of commercial viability.[33-35] We selected copper (Cu) as the scaffold material because it is highly conductive and cost-effective paired with high technical maturity, and because Cu surfaces favor the growth of dendritic structures applying electrodeposition method.

This paper has a twofold purpose: to understand how the electrodeposition process can be systematically adapted in order to tailor (i) the coverage and (ii) the catalytic properties towards CO_2RR of the deposited Ag catalyst. A complete coverage of the Cu foam with the Ag catalyst is vital to avoid Cu to take also part in the catalysis. The purpose of tuning the catalytic properties will be achieved by featuring crystallographic surface orientations that are conducive to selective CO production. Theoretical studies have proven that (110) and (220) Ag planes, respectively, particularly enhance the catalytic activity towards CO production.[36] It was shown that these facets facilitate the activation of CO_2 through a strong binding of the surface-adsorbed *COOH species (1st reaction step) before releasing CO due to weak binding of the *CO species (2nd reaction step). These findings, however, are supported only by a few experimental studies.[30,37] Therefore, the present study aims to further generalize the results by employing conventional and practical methods and materials to implement the desired crystallographic orientation of the catalyst surface at an industrial scale. The herein presented results evidence that the high active surface area of the Cu foam paired with the optimized facet orientations of the deposited Ag dendrites give rise to superior CO_2 conversion productivities, significantly enhancing the CO current density per area and mass, respectively, in comparison to other scaffold materials.

Overall the findings of this study provide a platform for the design of a highly active and selective cathode material for CO_2-to-CO conversion which can be employed in processes at large-scale industrial scale.

2. Experimental

2.1. Catalyst Deposition

The Ag catalyst deposition was conducted by an electrodeposition process on Cu foam employing a conventional electrochemical three-electrode set-up (VMP3 Bio-Logic multi-channel potentiostat). A sheet of Cu foam with a size of 40×40 mm^2 (2.5 mm thick, Recemat BV Cu-4753.04, average pore diameter: 0.4 mm) was used as the catalyst substrate (working electrode). Before the deposition, the foam was firstly cleaned in acetone, 2 M HCl, and deionized water. For the counter electrode a platinum mesh was used and Ag/AgCl/KCl (3M) (E^0=0.197 V_{NHE}) was used as reference electrode. The electrodeposition was conducted in a plating solution containing 0.1 M $AgNO_3$, 0.5 M NH_4OH, and 0.1 M NH_4NO_3.[38] The cathode optimization was performed by varying the deposition parameters at ambient conditions, i.e. the applied potential and the deposition time. The last cathode preparation step consisted in rinsing of the coated Cu foam with deionized water and drying at room temperature. The average Ag loading on the Cu foam was measured by weight difference. For comparison, silver and copper foils (Alfa Aesar, 99.998%, 0.1 mm thick) cathodes (with a mass of 104.9 g for 10 cm^2 of 0.1 mm Ag foil) and nickel (Ni) foam (1.4 mm thick, Recemat BV Ni-1116) were also employed.

2.2. Cathode Characterization

Experimental details on the structural (X-ray diffraction (XRD)), morphological (scanning electron microscopy (SEM), transmission and high resolution transmission electron microscopy (TEM and HRTEM)), and compositional (electron energy loss spectroscopy (EELS)) characterization methods applied herein to analyze the as-deposited Ag catalyst on the Cu foam have been provided in Ref. 39. X-ray photoelectron spectroscopy (XPS) was applied to analyze the electronic structure of the cathode surface by using a PHI instrument model 5773 Multitechnique with A1 Kα radiation (1486.6 eV).

The electrochemical performance of the Ag dendrite coated Cu foams towards CO_2 reduction was assessed using an adapted flow cell set-up (Micro Flow Cell, Electrocell A/S), which is schematically depicted in Figure 1 and which was already introduced as scalable (photo)-electrochemical device in our previous works.[39-41]

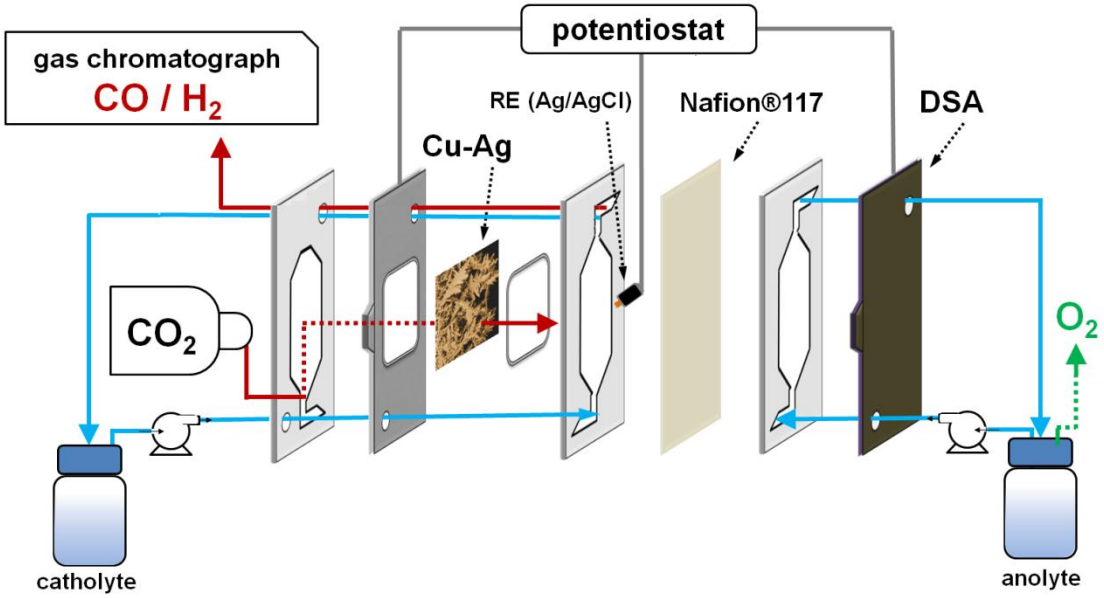

Figure 1. Sketch of the experimental set-up used to assess the CO_2RR performance of the Cu-Ag cathode. The set-up consisted of a filter-press flow cell with three inlets (catholyte, anolyte, and CO_2) and two outlets (catholyte + CO_2 and anolyte). Catholyte and anolyte compartments were separated by a Nafion membrane. The Cu-Ag cathode was mounted onto a metallic holder defining a geometric surface area of the cathode of 10 cm^2. The CO_2 gas and electrolyte pathways within the flow cell are indicated by the red and blue arrows, respectively. A 0.5 M $KHCO_3$ aqueous electrolyte solution (CO_2 saturated) was used as the electrolyte. The reference electrode was a Ag/AgCl (3.4 M KCl) electrode and a dimensionally stable anode plate (DSA) served as counter electrode.

The flow rates of CO_2 gas and electrolyte (0.5 M $KHCO_3$), respectively, within the flow cell were kept at 20 ml/min. As illustrated in Figure 1, the CO_2 gas was directly introduced through the macroporous 3D Cu-Ag foam cathode (geometric surface area: 10 cm^2). When using silver or copper foil, CO_2 was flown into the catholyte solution, as the gas, in this case, could not be injected directly through the cathode, which may affect the CO_2RR under operation in comparison to direct flow through the cathode. For details on the cyclic voltammetry (CV) and gas chromatography (GC) regarding the assessment of current-voltage behavior and the faradaic efficiency for gaseous CO_2RR

products, respectively, the reader is referred to Ref. 39 and the Supporting Information (SI), respectively.

3. Results

3.1. Catalyst deposition and characterization

We initiated our study with the coating of Cu foam substrate with Ag dendrite catalysts by means of electrodeposition. In the potentiostatic electrodeposition process, we investigated the effect of two parameters on the coating of the Cu foam: the deposition time and the applied potential. Figure 2 compares the morphologies of Ag coating on Cu foams after 15, 30, and 60 seconds at constant potentials of -0.05, -0.2, -0.35, and -0.5 V_{RHE}, respectively in the plating solution. At the lowest deposition potential (-0.05 V_{RHE}), the Cu foam surface was barely coated with Ag after 15 s and 30 s, respectively. After 60 s a continuous film of Ag started to grow but the dendrite structure was not observed at this applied potential. The electrodeposition at -0.2 V_{RHE}, on the contrary, led to a thin coating film with small dendrite like structures, with average dendrite sizes below 1 µm. However, after 15 and 30 s of deposition relatively large parts of the surface of the Cu substrate were still exposed and presumably accessible to the electrolyte. As a direct consequence, the Cu foam substrate, in this case, could also be active in the CO_2RR catalysis, which would be to the detriment to CO_2-to-CO conversion efficiency, because Cu surfaces are known to catalytically promote liquid chemicals as CO_2 reduction products, such as formic acid and methanol.[42] A high CO selectivity therefore requires an excellent coverage of the Cu foam with the Ag catalyst. The SEM image of the 60 seconds electrodeposition process revealed that the coverage of the foam substrate significantly augmented along with an increase of the Ag dendrite structure size. The dendrite branches ranged from 500 nm to 3 µm (or even bigger for a few distinct structures as observable in the respective quadrant in Figure 2) featuring a highly random coating of high surface area catalyst structures, which is conducive to the exposure of more active sites for CO_2RR and permeation of the catholyte. As apparent from Figure 2, the coating for -0.35 V_{RHE} applied potential, in average, led to bigger dendrite structures (branches and stem) for the respective deposition times. However, the coverage of the Cu foam seemed to be less dense compared to the one at -0.2 V_{RHE}. Both observation were confirmed for the deposition at -0.5 V_{RHE}, as the dendrites increased in dimension but significant portion of the Cu foam surface remained uncovered also after 60 s of deposition. This tendency was related to mass transport limitation of Ag ions at the electrode surface under increasing negative deposition potentials. As a result, existing dendrites continued growing, rather than new nucleation, and thus fewer dendrites appeared. Consequently, in this case, the coverage of the Cu foam was reduced.

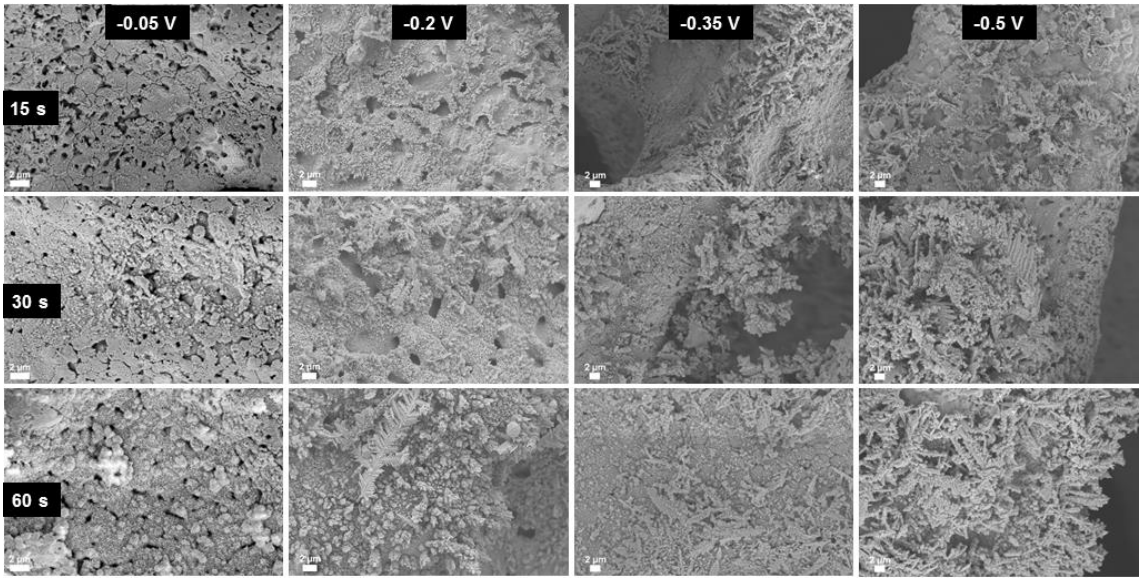

Figure 2. SEM images of the Ag dendrite catalyst electrodeposited on Cu foam for 15, 30, and 60 seconds at constant potentials of -0.05, -0.2, -0.35, and -0.5 V_{RHE}, respectively in the 0.1 M $AgNO_3$ containing plating solution.

Besides the analysis of the morphologies, shown in Figure 2, in general it is also important to determine the active surface area of the catalyst coated scaffold. For this purpose, we estimated the electrochemical active surface area (ECSA) for one of the Ag dendrite coated Cu foams in comparison to the ECSA of bare Cu foam. In fact, the ECSA can be estimated from the electrochemical double-layer capacitance C_{dl} at the solid/liquid interface.[25,27] The ECSA calculation process is presented in detail in the SI. From Figure S1a and S1b it can be deduced that the Ag dendrite coated Cu foam cathode exhibited a higher C_{dl} than bare Cu foam, evidencing a significantly higher active surface area, which was estimated as 92.50 cm^2 for the Ag dendrite coated Cu foam and 30.25 cm^2 for the bare Cu foam (tested geometric surface area for ECSA: 2 cm^2).

The next step in the investigation consisted in the analysis of the structural surface properties of the deposited Ag catalyst on Cu foam. The crystalline structure of the as-deposited Ag dendritic structures was investigated by XRD. Figure 3a exemplarily shows the XRD diffraction pattern for the sample deposited for 60 s at -0.2 V (see Figure 2). No significant differences in the XRD measurements were detected between the other prepared samples in Figure 2. The analysis revealed that the Ag dendrite electrocatalyst mainly crystallized in the cubic phase, while a small percentage of the hexagonal phase was measured as well (< 10%). The diffraction peaks are in perfect agreement with the reference pattern for cubic Ag (*JCPDS card number 00-001-1164*), namely Ag (111) at 38.1º, Ag (200) at 44.3º, Ag (220) at 64.5º and Ag (311) at 77.4º. The Ag (101) peak (*) corresponds to the hexagonal Ag phase with primitive lattice (*JCPDS Card number 00-041-1402*). The peaks from the Cu foam substrate corresponding to the Cu (*JCPDS card number 01-070-3038*) were also discernible in the diffraction pattern of the Cu-Ag system, as expected (Cu (111) at 43.2º, Cu (200) at 50.4º and Cu (220) at 74.1º).
Figure 3b plots the XPS spectrum of Ag $3d_{3/2}$ and Ag $3d_{5/2}$ double peaks from the substrate (again sample deposited for 60s at -0.2 V), which were centered at 374.3 and 368.3 eV, respectively. This was in perfect agreement with those of elemental Ag,[43,44]

and demonstrates that there was no corrosion of Ag dendrites during the electrodeposition procedure.

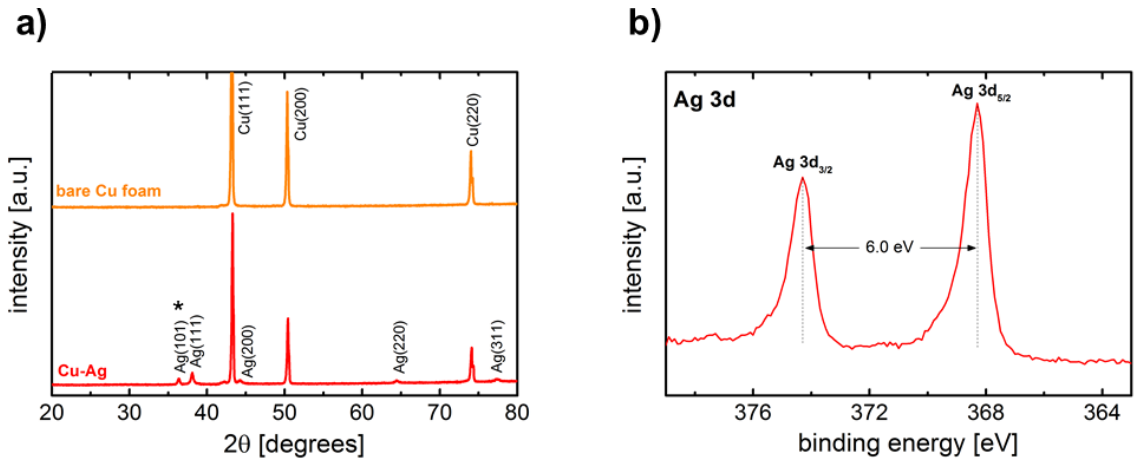

Figure 3. a) XRD measurements of the bare Cu foam (as reference for substrate material) and of the Ag coated Cu foam (Cu-Ag) showing signals stemming from hexagonal (*) and cubic phase Ag deposited at -0.2 V for 60 s. b) Respective high-resolution XPS analysis of Ag 3d spectrum for the Cu-Ag sample.

The deposited Ag dendrites were further investigated by means of high resolution TEM (also for sample deposited at -0.2 V for 60 s). Figure 4a displays the HRTEM image of one analyzed dendrite edge. The shape of the edge was random without sharp exposure to crystalline planes, indicating the random faceting planes of the dendrite structures. The highly crystalline feature of the Ag catalyst is persuasively depicted in Figure 4b. The fast Fourier transform (FFT) spectrum in Figure 4c (red squared region in Figure 4a) indicates that the edge nanostructures crystallized in the Ag cubic phase. The XRD measurement (Figure 3a), however, also identified a small hexagonal phase contribution. In this regard, Figure S2a in the SI shows the HRTEM image of a different dendrite edge, from which a polytypic behavior is observable. In these dendrites, periphery regions could be detected that presented many defects, such as twins and stacking faults. The FFT of Figure S2b furthermore reveals that there were two sets of diffraction patterns from the twinning domains (cubic), which shared the same planes of {1-11} (indicated by the white arrow in Figure S2a). The presence of a high density of twins, as those reported in Figure S2a, may induce the formation of polytypic structures, with alternating cubic and hexagonal domains in the nanostructure, as already typically observed in semiconductor nanostructures (e.g. Si,[45] GaAs,[46] ZnTe,[47]). In fact, this could be the origin of the cubic and hexagonal signals observed in the XRD patterns (Figure 3a).

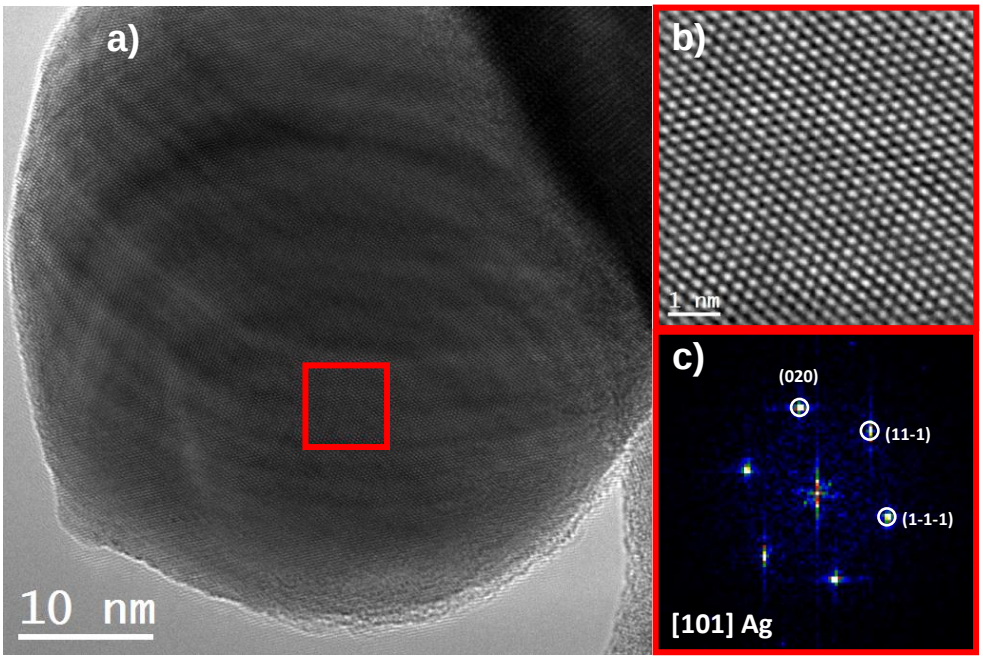

Figure 4. a) HRTEM image of the edge of a dendrite branch showing its structural distribution. b) HRTEM detail of the red marked region in a). c) The corresponding temperature colored FFT spectrum of the red squared region indicating that the material in the dendrite branch crystallizes in the cubic Ag phase, [FM3M]-Space group 225, with lattice parameters of a = b = c = 0.4164 nm, and α = β = γ = 90° as visualized along the [101] direction.

The crystallographic orientation of the dendritic structures was assessed hereafter. The low magnification view of the Ag-Cu foam samples in Figure 5a shows the dendritic structure comprising the stem and the dendrite branches. As apparent from Figure 5a), the branches followed <111> directions and an angle between the stem and the branches of 109.5º could be measured. This implies that the stem of the Ag dendrites grew along the [001] direction. Based on this finding and based on the FFT result shown in Figure S2b, a simulated diffraction pattern (inset in Figure 5a) could be deduced. This information allowed performing a simulated scale model of the Ag dendrite branch along the [1-11] growth direction, shown in Figure 5b. and Figure 5c, respectively. The illustration nicely depicts the dendritic shape along with the main and secondary surface facet types, {110} and {112}, respectively (Figure 5d). Such facet-rich structures can boost the CO_2-to-CO conversion rates, as shown previously for Ag and Au nanostructures, respectively, and thus, are of particular interest for the herein targeted CO production.[20,48,49]

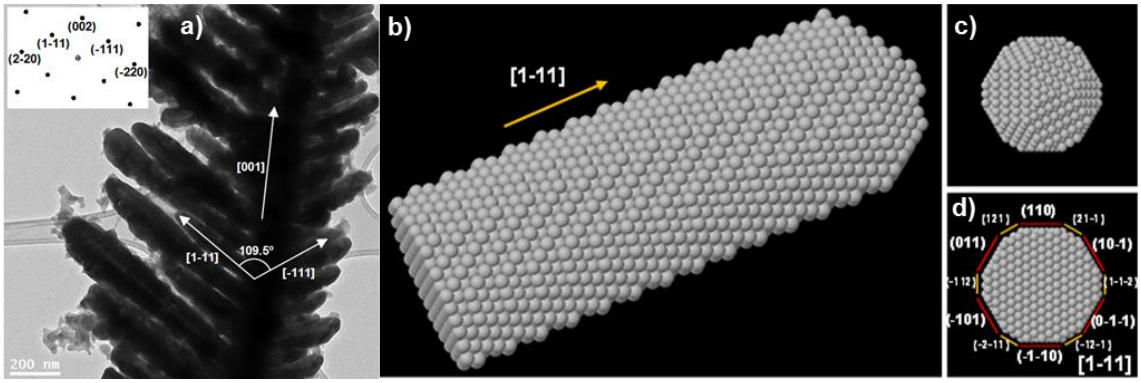

Figure 5. a) Low magnification TEM image of the Ag-Cu foam sample showing the dendritic shape with the crystal directions labeled. The inset corresponds to a simulated diffraction pattern in agreement with the FFT results shown in Figure S2b. b) Simulated scaled model of an Ag dendritic branch along the [1-11] growth direction, as found by HRTEM. c) Front view of the dendrite branch showing the rounded tip terminated in a (1-11) facet. d) Dendrite branch cross section showing the lateral facets, with main {110}-type surfaces (marked in red) and secondary {112}-type facets (marked in yellow).

To investigate the dendrite structural composition in more detail, EELS spectrum images (compositional maps) were obtained at the nanoscale. The acquired composition map of an Ag dendrite branch is shown in Figure 6. The analysis evidenced that the dendrite branches were mainly composed of crystalline Ag, which dominated the core part of the catalyst structures. In the thin periphery region, oxygen, copper, and carbon were detected. The latter element was detected as residual from the hexane dispersion solution (see Experimental 2.2), while Cu may have occurred from the residual of Cu foam in the dispersion solution used for the TEM measurements (see Experimental 2.2). The evidenced oxygen is supposed to stem from the oxidation of copper and carbon residuals because the crystalline Ag dominates the dendritic matrix based on the HRTEM characterization. Therefore, we can assume that the residual induced periphery layer (down right in Figure 6) was not present in the as-deposited Ag catalyst structure, and thus would not affect the electrochemical characterization.

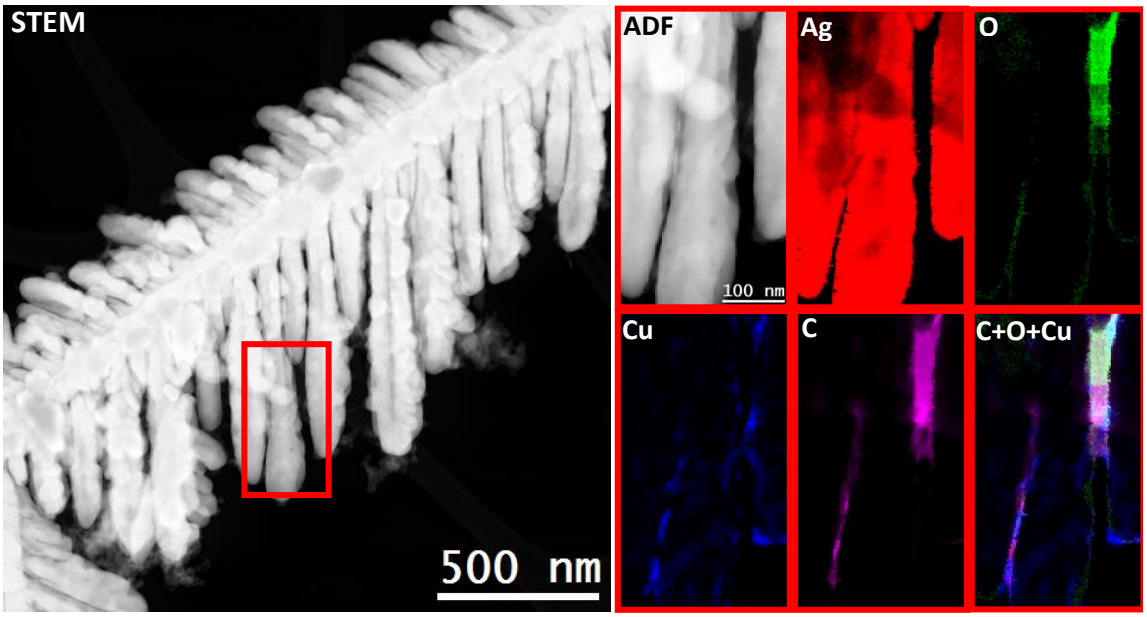

Figure 6. Left: General annular dark field (ADF) STEM image of a dendrite branch. Right: Nanoscale EELS chemical composition maps obtained from the red rectangled area on the ADF-STEM micrograph. Individual Ag (red), O (green), Cu (blue), C (pink) maps and their composite.

3.2. Electrochemical reduction of CO_2

The electrochemical performance of the Cu-Ag cathodes regarding CO_2RR was assessed in the electrochemical flow cell (three-electrode configuration), as shown in Figure 1. A commonly employed 0.5 M $KHCO_3$ aqueous electrolyte solution saturated with CO_2 (pH = 7.5) was used as catholyte.[21,24,26,29] The fluidic characteristics of the employed cell design allowed to recirculate the catholyte solution (flow rate of 20 ml/min), while the CO_2 gas was directly injected through the macroporous 3D Cu-Ag

cathode. Such continuous-flow operation designs allow alleviating mass transport limitations for CO_2RR catalysis and thus improving partial current densities of reaction products, as shown by Kenis et al. and Newman et al.[50,51] In one of our prior studies, we identified a gas-to-electrolyte flow ratio of 1 as optimum for the flow reactor design, which is why we also employed this ratio in the present study. In particular, it was verified that a ratio of 1 ensures the perfect balance between offering the right amount of catholyte and CO_2 gas at the cathode surface.[40]

Figure 7 depicts the faradaic efficiencies at different potentials achieved with the Cu foam cathode prepared at -0.2 V_{RHE} for 15, 30, and 60 s electrodeposition of Ag. An electrodeposition time of 0 seconds refers to bare Cu foam. The calculation of the faradaic efficiencies of CO and H_2 is described in detail in the SI.

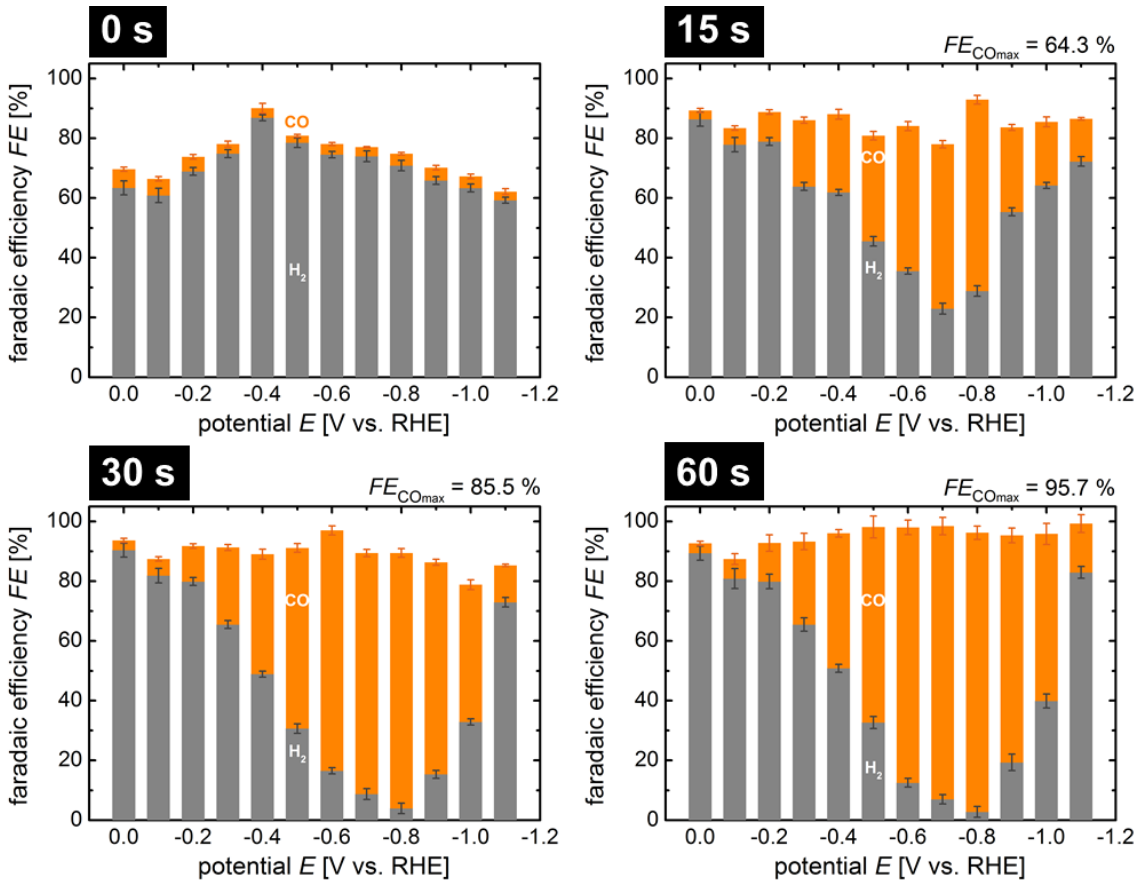

Figure 7. Faradaic efficiencies of CO and H_2 production as a function of the applied potential for the cathodes prepared at -0.2 V_{RHE} (see Figure 2) with the according Ag electrodeposition time indicated. The error bars indicate standard deviations obtained from 2 experimental repeats. A flow rate of 20 ml/min was applied for the CO_2 and electrolyte flow, respectively. The respective maximum CO faradaic efficiencies for Ag dendrite coated Cu foam cathodes are indicated above the insets.

As expected, the bare Cu foam surface (0 seconds of electrodeposition time) did not promote the generation of CO. The data shows that H_2 was the major detected gaseous product with a maximum faradaic efficiency of 87.8 % at -0.4 V_{RHE}. The selectivity for CO production was below 5 % for the entire investigated potential range and the total faradaic efficiency for CO and H_2 ranged between 61 % and 91 %. This suggested the formation of other products (not measured here), for instance formic acid, as already reported elsewhere.[42]

The thin coating film provided after 15 seconds of electrodeposition immensely affected the catalytic behavior of the tested cathode, as the selectivity towards CO products drastically increased (Figure 7, upper right). The CO faradaic efficiency significantly augmented for the majority of the investigated potentials from around 5 % without Ag dendrites (0 s) to a maximum value of 64.3 % at -0.8 V_{RHE} for the Ag dendrite coated Cu foam cathode (15 s). However, the total faradaic efficiency remained between 81 % and 90 % for the different potentials, suggesting that the uncovered Cu foam areas take part in the CO_2RR catalysis to produce other products (as expected and shown in Ref. 42). A more dense coverage of the Cu foam including increased dendrite structures, which was obvious after 30 seconds of electrodeposition (see Figure 2 for -0.2 V_{RHE}), further drastically increased the selectivity towards CO formation, as can be seen from the lower left plot in Figure 7, with a maximum faradaic efficiency of 85.5 % (at -0.8 V_{RHE}). This entails that the total faradaic efficiency for CO and H_2 surpassed 90 % for the majority of the investigated potentials and reached values up to 97 %. The best selectivity for CO and H_2 was however exhibited by the cathode prepared for 60 s (at -0.2 V_{RHE}, Figure 2). As apparent from the lower right graph in Figure 7, CO production was amplified for all investigated potentials, especially in the potential range between -0.4 and -1.1 V_{RHE}. In this range, total CO/H_2 faradaic efficiencies close to 100 % were measured along with a maximum CO faradaic efficiency of 95.7 % at -0.8 V_{RHE} applied bias, implying an excellent coverage of the Cu foam with the Ag dendritic catalyst. For lower potentials (< -0.4 V_{RHE}) we expect the formation of low amounts of liquid products (not measured here), as already reported elsewhere for Ag catalysts.[29] Deposition times beyond 60 s were also considered in this study. In the SI, the morphology and the faradaic efficiency of the Cu foam cathode, respectively, after 2 and 3 min of electrodeposition are shown (Figure S3). As apparent the coating of the 3D foam was highly dense in both cases. Additionally the overall selectivity towards gas production (CO + H_2) slightly increased, and reached nearly 100 % faradaic efficiency in the investigated potential range. However, the maximum faradaic efficiency for the targeted CO (in both cases at -0.8 V_{RHE}) could not be augmented (94.7 % and 92.3 %, respectively).

Figure 8 depicts the maximum CO faradaic efficiency (FE_{CO}) as a function of the electrodeposition time and the applied potential in the potentiostatic process for all investigated samples (shown in Figure 2). This graph enables to examine the impact of the complete set of parameters on the catalytic performance studied in this work. The values for maximum faradaic efficiency in Figure 8 were acquired at -0.8 V_{RHE}, as the highest CO selectivity was detected at this cathodic potential for the samples deposited at -0.2 V (see Figure 7). From Figure 8 it becomes obvious that, except for the -0.05 V samples (grey triangles), deposition times beyond 60 s could not lead to higher maximum CO selectivities. The values for FE_{CO} did not increase (even decreased slightly) for longer deposition times for the cathodes deposited at -0.2 (black squares), -0.35 (purple circles), and -0.5 V_{RHE} (blue diamonds), respectively. This observation suggests that after 60 s no new nucleation could start (because of complete coverage or ion diffusion limitation) and that prolonged deposition times solely increased the dendrite dimensions. Hence the CO selectivity was slightly impaired, as it is well accepted that nano/microsized catalysts propel catalytic activities more than macroscopic structures.[3]

We therefore concluded that plating processes longer than 60 s are not beneficial for this process with respect to high CO selectivity. Moreover, this result was in line with the aim to minimize process time and loaded catalyst material in view of large scale commercial application. The highest faradaic efficiency measured in this study was 95.7

% for the Cu-Ag cathode deposited at -0.2 V for 60 s. Furthermore, our flow cell device design allows for advanced flow dynamics, which results in lower potentials to reach such high selectivity compared to related CO_2RR systems. To estimate

In the following we focus on the comparison of Cu foam with other catalyst substrates, such as foils of Cu and Ag and Ni foam. By checking Cu foam against other catalyst scaffolds, we expect to gain a better understanding of the catalytic activity towards CO_2RR, especially regarding the effect of the deposited catalyst morphology and structure.

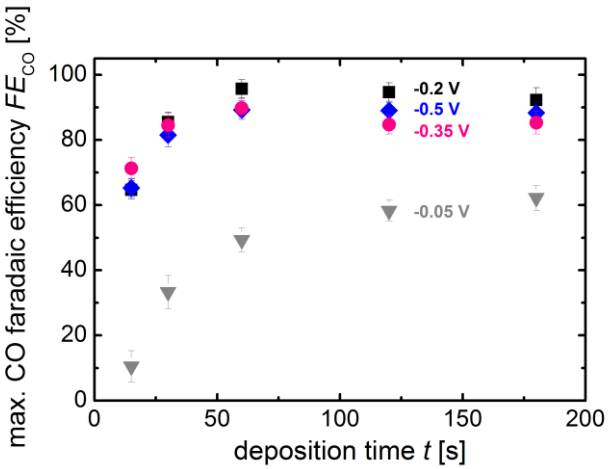

Figure 8. Maximum faradaic efficiency for CO production as a function of the deposition time and the applied potentials during the potentiostatic electrodeposition process. The error bars indicate standard deviations obtained from 2 experimental repeats. A flow rate of 20 ml/min was applied for the CO_2 and electrolyte flow, respectively. The values were acquired at an applied potential of -0.8 V_{RHE}.

3.3. Comparison of Cu Foam with Other Substrates

Figure 9a represents the cyclic voltammogram of the champion Cu foam based cathode (deposited at -0.2 V for 60 s) from Figure 7 and Figure 8 (black curve). For comparison, the same measurement was also conducted for a flat Cu foil with Ag catalyst (green curve) and a flat Ag foil cathode (orange curve). The Cu foil sample was coated with Ag employing the same electrodeposition process as for the Cu foam cathode. As apparent from the SEM image shown in the SI, in Figure S4a and S4b, the same deposition process did not lead to the growth of dendritic structures on Cu foil, but to Ag agglomerates. Fluctuations in the CV curves may stem from the characteristics of the used flow-reactor set-up.

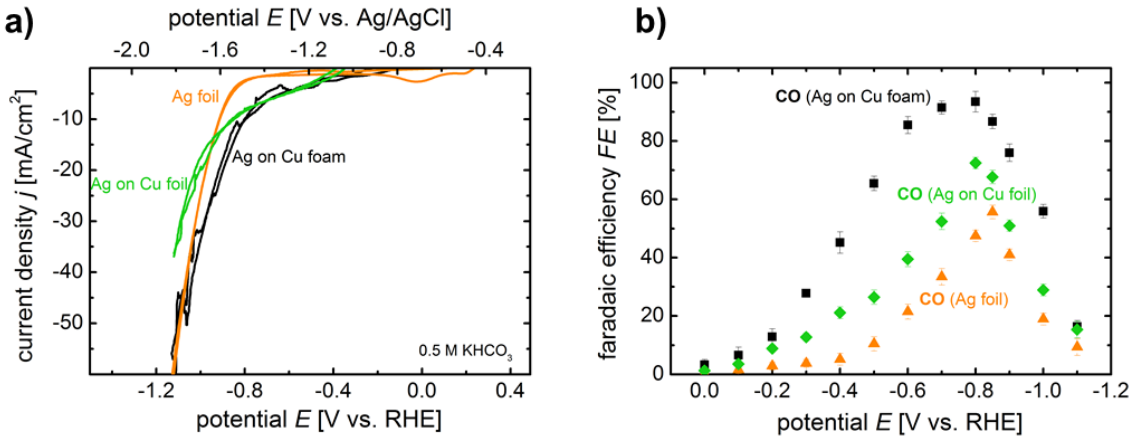

Figure 9. a) Cyclic voltammetry measurements of the Ag dendrite coated Cu foam cathode (black curve). For comparison the CV measurements of an Ag foil (orange curve) and a Cu foil coated with Ag (green curve, same Ag deposition parameters as for the Cu foam). All the measurements were conducted in 0.5 M $KHCO_3$ at a scan rate of 10 mV/s. The current densities are based on geometric cathode surface areas (10 cm^2). The steady state CVs were obtained after three cycles. b) Faradaic efficiencies of CO for the Ag dendrite catalyst coated Cu foam cathode (black squares), for the Ag foil cathode (orange triangles) and for the Cu foil cathode (green diamonds) at different potentials. For the Ag and Cu foil electrodes, CO_2 was bubbled in the catholyte solution (see Section 2). The error bars indicate standard deviations obtained from 2 experimental repeats. A flow rate of 20 ml/min was applied for CO_2 and electrolyte flow, respectively. The corresponding faradaic efficiencies of H_2 for the investigated samples are shown in Figure S6 in the SI.

For the Ag foil, it can be seen from Figure 9a that no evident voltammetric response was detected before the potential -0.6 V_{RHE}, indicating the negligible CO_2RR activity. Inversely, the CO_2RR current of the Ag dendrite coated Cu foam appeared at the earliest potential of -0.3 V_{RHE} owing to its large catalytically active 3D surface and the direct injection of gaseous CO_2 at the cathode surface, which favors the CO_2RR kinetics. The onset potential measured for the Cu foil coated with the Ag agglomerates was around -0.4 V_{RHE}. From Figure 9a it can therefore be concluded that the performance of the Ag coated Cu foam cathode exceeded the performance of the Ag foil and Cu-Ag foil regarding CO_2RR current density in the entire investigated potential range from 0 to -1.0 V_{RHE}. Only for potentials above -1.0 V_{RHE} the Ag foil and Cu-Ag foam cathode provided similar current densities. The superior electrochemical performance of the Ag coated Cu foam cathode regarding CO_2RR was further evidenced by comparing the performance of the sample measured under pure argon (Ar) flow. As apparent from Figure S5, the cathode performance was significantly enhanced under CO_2 flow compared to Ar flow, regarding onset potential for cathodic current and high current densities.

Following the CV measurement, we subsequently assessed the CO_2RR selectivity of the Cu-Ag foam cathode and of the two other electrodes towards reaction products using gas chromatography. Figure 9b displays the measured faradaic efficiencies for CO which were already presented in Figure 7 for the 60s sample. CO and H_2 partial current densities of the CO_2RR are plotted in Figure S7. As already apparent from Figure 7 (for 60 s), a very high selectivity for the generation of the two gaseous products CO and H_2 was exhibited from the Cu-Ag foam cathode (total faradaic efficiency close to 100 % for potentials from 0 to -1.1 V_{RHE}, see Figure 9b and Figure S6). At the highest faradaic efficiency of CO of 95.7 % (at -0.8 V_{RHE}) this cathode exhibited an eminent CO current density of 9.5 mA/cm^2 (Figure S7). A maximum CO partial current density of 27.3

mA/cm^2 was measured at -1.0 V_{RHE}. Further increase in applied potential did not result in higher CO yield because mostly H_2 formation was promoted (see black squares in Figure S6). Similar observations in other reports were assigned to mass transport limitations of CO_2 at high current densities and not to the intrinsic activity of the Ag catalysts.[19,52] Nevertheless, the herein demonstrated CO production yield (at low potentials < -1.0 V_{RHE}) surpasses the performance of Ag dendrite and other Ag based systems for CO_2RR at ambient conditions.[20,29,30,51,53,54] Therefore, our findings clearly demonstrate the superior electrochemical characteristics of the presented metallic foam supported cathode.

Figure 9b furthermore provides evidence that the Ag dendrite based foam cathode outperformed the Ag and Cu foil scaffold cathode with respect to selectivity for CO production. The CO faradaic efficiencies measured for the Ag foil (orange triangles) and Cu foil (green diamonds), respectively, were below the values of the Cu-Ag cathode (black squares) in the entire investigated potential range with an inferior maximum faradaic efficiency of 55.7 % and 72.5 %, respectively (both at -0.8 V_{RHE}). Notably from Figure 9b, the CO selectivity of the Cu foam based cathode also started to augment at lower potentials than for the Ag and Cu foil based cathodes, respectively. This behavior exactly mirrors the respective CV curves in Figure 9a, i.e. the shift in the onset potentials for CO_2RR of both tested cathodes. In fact, the enhanced CO_2RR catalytic activity can be ascribed to the combination of nano/microsized dendrites with the 3D macroporous structure of the supporting Cu foam itself. This marriage resulted in a significantly increased contact area between catalysts and electrolytes and provided a greater amount of active sites where CO_2RR could take place (see ECSA estimation in the SI, Figure S1). Furthermore, the flow cell design of the applied reactor ensured an improved transport of reactants (CO_2 and electrolyte) and products (CO and H_2). Moreover, the presented Ag dendrite catalyst offers distinct advantages regarding large scale applications due to its facile deposition and high catalytic performance in delivering significantly higher (4 orders of magnitude) mass specific CO current density than flat Ag foil (see corresponding plot in Figure S8).

Besides CV and GC data, another crucial parameter of electrocatalytic activity is the corresponding Tafel slope. In Figure 10 the logarithm of the CO partial current density is plotted against the potential of the Ag dendrite coated Cu foam and Ag foil cathode. The Tafel slope is acquired from the range of linearity at the low-voltage scope. As listed in Figure 10, in this region, the Tafel slope of Cu-Ag cathode was 89.7 mV/dec, and thus, as expected, much lower than Ag foil (198.7 mV/dec) and also lower compared to other Ag structures for CO_2RR.[20,26] This result verifies that the Ag dendrite catalyst promotes a fast CO_2RR rate. The high-current data in Figure 10 reflects the data shown in Figure S7 and evidences that the Cu-Ag foam cathode, in this region, exhibited much higher CO production current densities than the flat Ag foil. The observable decay in the CO production was caused by an increase of the hydrogen production and occurred at lower potentials in the case of the Ag foil, preventing a better catalytic performance.

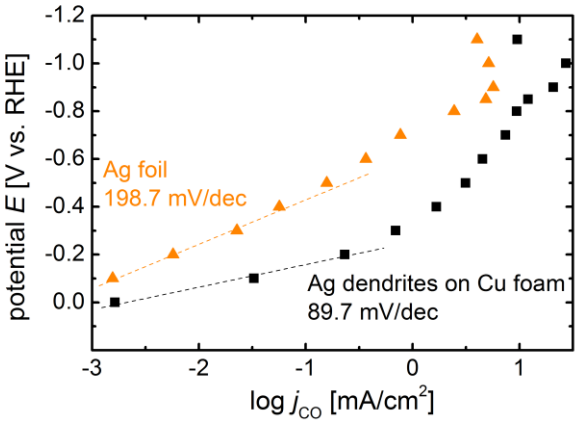

Figure 10. Applied potential versus CO production partial current density for Ag dendrites (black squares) and Ag foil (orange triangles).

In particular, the Tafel evaluation gives insights in the CO_2RR reaction kinetics. It is well accepted that the first step of the reaction consists in the transfer of one electron to a CO_2 molecule to form a CO_2 radical absorbed on the catalyst surface. This step is rate determining for the entire reaction process, because it proceeds (as suggested by literature) at much more negative potentials than subsequent steps, in which the CO_2 intermediate species reacts with two protons and another electron to form a CO and a H_2O molecule. The much lower Tafel slope for the Ag dendrite based cathode, as depicted in Figure 10, therefore suggests that the Ag dendrite surfaces are able to stabilize the CO_2 intermediate more efficiently than a flat surface, and thus propel the formation of CO molecules subsequently. This observation is of highest importance for CO production and was already studied theoretically and experimentally, respectively.[36,37]

Durability is a vital appraisal criterion to estimate a practical electrolysis application. Figure 11 displays the examined long-term stability of the Ag dendrite coated Cu foam cathode integrated in our flow cell reactor. For comparison, the potentiostatic measurement of the Ag foil was also included. At an applied potential of -0.8 V_{RHE} (potential of maximum FE_{CO}), the Cu-Ag cathode exhibited a current density of around 10 mA/cm^2 which stabilized around this value over the whole reaction session, without the observation of a significant decay (95% retained after 15 hours of continuous operation). Similarly, the CO faradaic efficiency was also stabilized around 94 % for the whole duration of 15 hours of testing. Measured current density and faradaic efficiency are in accordance to the data presented in Figure S7 and Figure 9b, respectively. Thus, the stability of our prototype reactor was in good agreement with previously reported stabilities for Ag catalyst based electrodes.[21,29] The operation robustness of the Cu–Ag cathode was additionally confirmed by SEM, TEM, and XRD analysis, respectively (see Figure S9, in the SI). As presented in Figure S9a and S9b, the Ag dendrites preserved their morphology and structural properties, respectively, after long-term electrolysis at -0.8 V_{RHE}. The XRD diffraction peaks were identical before and after the 15 hours electrolysis operation (Figure S9c). For the sake of completeness, we also assessed the stability of the Ag foil (Figure 11), which, as expected, also exhibited a very stable operation (tested for 5 hours) with a lower CO_2RR current density of around 3.4 mA/cm^2 and a CO selectivity of around 41 %, which was in line with the data shown in Figure 9a and 9b, respectively.

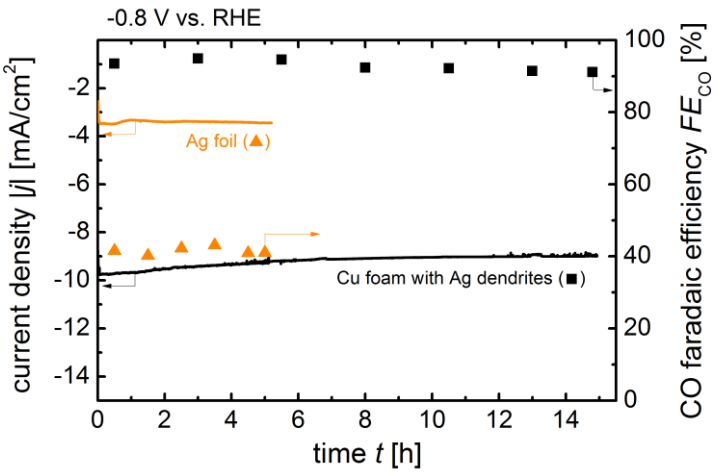

Figure 11. Stability of total CO_2 reduction current density (left ordinate) for Ag dendrites (black curve and squares) and Ag foil (orange curve and triangles) at -0.8 V_{RHE} in 0.5 M $KHCO_3$. The CO faradaic efficiency of both tested cathodes as a function of operation time is plotted on the right ordinate.

Besides the comparison with flat metallic foil surfaces, the Cu foam was also checked against a Ni 3D metallic foam, as high surface area catalyst scaffold. Two-dimensional scaffold materials, such as carbon cloth or titanium mesh were not investigated in the present study, mainly because of the lower surface area and lower electrical conductivity compared to Ni foam.[55,56] In the SI, the comparison with Ni foam, regarding Ag catalyst deposition and selectivity towards CO production is presented. In contrast to the Cu foam surface, the Ni foam surface did not give rise to dendritic catalyst growth, but the Ag catalyst was deposited in the form of particles of 1 µm in average (see SEM images in the SI, in Figure S10a and Figure S10b). The results on partial CO and H_2 current densities, respectively, presented in Figure S11, furthermore evidence that the Cu-Ag cathode showed a significantly higher selectivity towards CO production than the Ni-Ag cathode, which confirms the outstanding performance of the developed Cu-foam based cathode.

4. Discussion

The reason for the discrepancy in the activity towards CO production between the investigated cathodes, observable in Figure 9b and Figure S11, respectively, can be explained by several factors. (i) First, the morphology of the deposited Ag catalyst is a crucial parameter regarding CO_2 conversion activity. Based on the SEM images it can be deduced that the dendritic structures showing the highest activity towards CO production (i.e. deposited for 60 s at -0.2 V_{RHE}, Figure 2) possessed more active surface area compared to the other Ag catalyst morphologies obtained on Cu foam (e.g. deposition at -0.05 V_{RHE}, Figure 2), Cu foil (Figure S4b) and Ni foam (Figure S10b). (ii) Secondly, the better coverage of the Cu foam with the dendritic catalysts (see deposition at -0.2 V_{RHE} in Figure 2 and Figure 6) ensured that only the Ag catalyst was active in the CO_2RR. As explained earlier, surfaces such as Cu and Ni favor other products than CO. Cu favors alcohol production and Ni surfaces are known to favor the hydrogen evolution reaction. The latter is in line with the data on partial current density shown in Figure S11, which reveals that the Ni-Ag sample showed a higher activity towards H_2 production than the Cu-Ag sample. (iii) Another important parameter influencing the

CO_2RR activity towards CO is the catalyst surface morphology. As revealed by experiment and simulation (Figure 5), the as-deposited Ag dendrites had a high number of planes. It is well accepted that (110) planes own a high amount of stepped sites, which are highly active sites for CO_2-to-CO conversion.[36,37,49] To directly measure the ratio of (110) planes vs. more flat sites is however very challenging for 3D materials in general. To quantify the relative amount of (110) surface, a more convenient approach would be to calculate the ratio of (110) and (111) intensities with the help of XRD measurements. Please note that the diffraction peak of Ag (110) was not observable in the XRD pattern of the Cu-Ag foam (Figure 3a) because in face centered cubic structures this reflection is not allowed. Nevertheless, it can be assumed that the (110) structure exists in an amount proportional to that of (220). Consequently, we took the ratio of the Ag signals (220)/(111) as approximation for the quantity of stepped vs. planar sites, as already described elsewhere.[30] In Figure 12, the values for the intensity ratios for four investigated samples are plotted as a function of the respective maximum CO faradaic efficiency. The comparison was conducted for four samples owing different morphologies of the deposited Ag catalysts: Ag dendrites deposited on Cu foam (for 60 s at -0.2 V_{RHE}), which will be called "optimized" hereafter, because the highest CO productivity was achieved with this sample (morphology: Figure 2 and faradaic efficiency: Figure 8); Ag catalyst deposited on Cu foam (for 60 s at -0.05 V_{RHE}), which will be called "non-optimized", because the corresponding CO productivity of this sample was significantly below the optimized one (morphology: Figure 2 and faradaic efficiency: Figure 8); Ag catalyst deposited on Cu foil (morphology: Figure S4b and faradaic efficiency: Figure 9b) and Ag catalyst deposited on Ni foam (morphology: Figure S10b, CO productivity: Figure S11). Ag on Cu foil and on Ni foam, respectively, was deposited with the same deposition process as for the optimized sample.

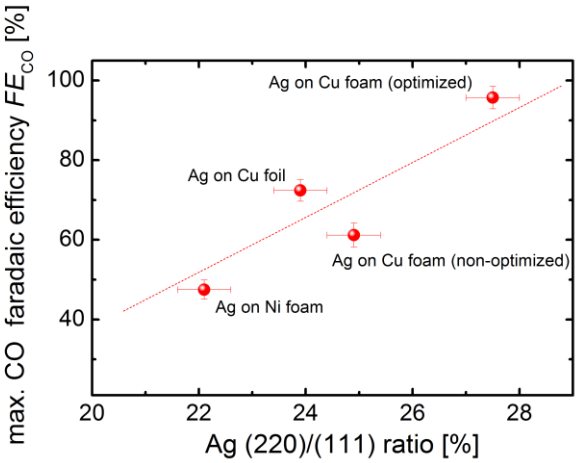

Figure 12. Maximum CO faradaic efficiency (FE_{CO}) as a function of the (220)/(111) intensity ratio of the deposited Ag catalyst obtained from the GC and XRD measurements, respectively, for four investigated samples: Ag deposited on Cu foam (60 s at –0.2 V, optimized), Ag deposited on Cu foam (60 s at -0.05 V, non-optimized), Ag deposited on Ni foam (60 s at -0.2 V) and Ag deposited on Cu foil (60 s at -0.2 V). The error bars indicate standard deviations obtained from 2 experimental repeats (y-axis) and account for inaccuracy in ratio determination from XRD patterns in Figure S12 (x-axis).

From the data in Figure 12, a clear trend of increasing FE_{CO} with increasing (220)/(111) ratio can be deduced. The XRD measurements from which the (220)/(111) ratios are deduced, can be found in the SI in Figure S12.

As apparent, the optimized Ag dendrite catalyst on Cu foam, exhibiting the highest FE_{CO} of 95.7%, also showed the highest (220)/(111) intensity ratio of 27.5%. The lowest ratio of 22.1% was found for the Ag catalyst deposited on Ni foam, for which also the lowest FE_{CO} among the investigated samples of 47.5% was measured. Hence, the experimental findings of this study support the theoretical calculations done by Back et al. showing that Ag surfaces owing a high amount of (220) planes are prone to high CO productivity.[36] Overall, the present study successfully generalizes the theoretical findings on Ag catalyst behavior towards CO_2RR by employing practical concepts to implement the desired crystallographic orientations of the catalyst surface at large scale.

5. Conclusions

In summary, we successfully tailored large-scale metallic foam for highly selective CO_2 conversion into CO at high current and low overpotentials. The experimental observations manifested that the combination of Ag dendritic catalysts with highly conductive 3D Cu foam effectively ameliorated the electrocatalytic performance towards CO production and gave rise to a stable maximum faradaic efficiency of 95.7 % at -0.8 V_{RHE}. A maximum operation current density of 27.3 mA/cm^2 was measured at -1.0 V_{RHE}. The performance boost, in comparison with other catalyst substrates, was attributed to mainly two features of the Cu foam based cathode: (i) reduced mass transport limitations due to the amplified 3D electrochemically active contact area between the homogeneously coated Cu foam and the electrolyte and (ii) the demonstrated high selectivity of the deposited Ag catalyst towards CO production, which could be attributed to the unique dendrite surface orientations favoring a high density of active sites where CO_2RR to CO could take place (high (220)/(111) XRD intensity ratio). Overall, this work exploits a novel pathway for the fabrication and application of robust, efficient, and highly selective metallic foam based electrodes in prototype reactor devices, which are viable for scalable electrochemical reduction of CO_2 to CO at large scale.

Associated Content

Supporting Information:

Gas product quantification calculation; Electrochemical surface area (ECSA) estimation of Ag dendrite coated Cu foam; Comparison between Cu and Ni foam for the deposition of Ag catalysts; Additional structural and electrochemical characterization.

Acknowledgments

Authors acknowledge funding from Generalitat de Catalunya through the CERCA program, 2017 SGR 1246, 2017 SGR 327 and the Spanish MINECO projects MAT2014-59961, ENE2016-80788-C5-5-R and ENE2017-85087, together with the support from REPSOL, S. A.
ICN2 acknowledges support from the Severo Ochoa Programme (MINECO, Grant no. SEV-2013-0295). IREC also acknowledges additional support from the European Regional Development Funds (ERDF, FEDER), (S)TEM part of the present work has been performed in the framework of Universitat Autònoma de Barcelona Materials

Science PhD program and the rest in the Nanoscience program of the University of Barcelona.
Authors thank M. López Balastegui, M. Biset-Peiró and S. Murcia-López for their contributions to this work.
F.U. acknowledges financial support from MINECO through Juan de la Cierva fellowship (FJCI-2016-29147).

Author Contributions

F.U. and T.A. conceived the project and designed the experiments. F.U. carried out the structural and electrochemical experiments under the advisory task of T.A. and J.R.M. F.U. and N.M.C. performed the silver electrodepositions. P.Y.T. and J.A. conducted (S)TEM and EELS analyses. F.U. and J.R.M. interpreted data. F.U. wrote the manuscript. All authors participated in discussions and contributed to editing of the manuscript. J.R.M. supervised the proposed and executed research program.

Competing Financial Interests

The authors declare no competing financial interests.

References

[1] Goeppert, A.; Czaun, M.; May, R. B.; Prakash, G. K. S.; Olah, G. A.; Narayanan, S. R. Carbon Dioxide Capture from the Air using a Polyamine based Regenerable Solid Adsorbent
J. Am. Chem. Soc. **2011**, *133*, 20164.

[2] Schreier, M.; Gao, P.; Mayer, M.T.; Luo, J.; Moehl, T.; Nazeeruddin, M.K.; Tilley, S. D.; Grätzel, M. Efficient and Selective Carbon Dioxide Reduction on Low Cost Protected Cu_2O Photocathodes using a Molecular Catalyst
Energy Environ. Sci. **2015**, *8*, 855.

[3] Rosen, J.; Hutchings, G. S.; Lu, Q.; Rivera, S.; Zhou, Y.; Vlachos, D. G.; Jiao, F. Mechanistic Insights into the Electrochemical Reduction of CO_2 to CO on Nanostructured Ag Surfaces
ACS Catal. **2015**, *5*, 4293.

[4] Asadi, M.; Kim, K.; Liu, C.; Addepalli, A. V.; Abbasi, P.; Yasaei, P.; Phillips, P.; Behranginia, A.; Cerrato, J. M.; Haasch, R.; Zapol, P.; Kumar, B.; Klie, R. F.; Abiade, J.; Curtiss, L. A.; Salehi-Khojin, A. Nanostructured Transition Metal Dichalcogenide Electrocatalysts for CO_2 Reduction in Ionic Liquid
Science **2016**, *353*, 467.

[5] Zhou, X.; Liu, R.; Chen, Y.; Verlage, E.; Francis, S. A.; Lewis, N. S.; Xiang, C. Solar-Driven Reduction of 1 atm of CO_2 to Formate at 10% Energy-Conversion Efficiency by Use of a TiO_2-Protected III–V Tandem Photoanode in Conjunction with a Bipolar Membrane and a Pd/C Cathode
ACS Energy Lett. **2016**, *1*, 764.

[6] Wang, Y.; Fan, S.; AlOtaibi, B.; Wang, Y.; Li, L.; Mi, Z. A Monolithically Integrated Gallium Nitride Nanowire/Silicon Solar Cell Photocathode for Selective Carbon Dioxide Reduction to Methane
Chem. Eur. J. **2016**, *22*, 8809.

[7] Kuhl, K. P.; Hatsukade, T.; Cave, E. R.; Abram, D.N.; Kibsgaard, J.; Jaramillo, T.F. Electrocatalytic Conversion of Carbon Dioxide to Methane and Methanol on Transition Metal Surfaces
J. Am. Chem. Soc. **2014**, *136***,** 14107.

[8] Ren, D.; Deng, Y.; Handoko, A. D.; Chen, C. S.; Malkhandi, S.; Yeo, B.S. Selective Electrochemical Reduction of Carbon Dioxide to Ethylene and Ethanol on Copper (I) Oxide Catalysts
ACS Catal. **2015**, *5*, 2814.

[9] Qiao, J.; Liu, Y.; Hong, F.; Zhang, J. A Review of Catalysts for the Electroreduction of Carbon Dioxide to Produce Low-Carbon Fuels
Chem. Soc. Rev. **2014**, *43*, 631.

[10] Jin, G.; Werncke, C. G.; Escudié, Y.; Sabo-Etienne, S.; Bontemps, S. Iron-Catalyzed Reduction of CO_2 into Methylene: Formation of C–N, C–O, and C–C Bonds
J. Am. Chem. Soc. **2015**, *137*, 9563.

[11] Wender, I. Reactions of Synthesis Gas
Fuel Process. Technol. **1996**, *48*, 189.

[12] Schreier, M.; Curvat, L.; Giordano, F.; Steier, L.; Abate, A.; Zakeeruddin, S. M.; Luo, J.; Mayer, M. T.; Grätzel, M. Efficient Photosynthesis of Carbon Monoxide from CO_2 using Perovskite Photovoltaics
Nat. Commun. **2015**, *6*, 7326.

[13] Jang, Y. J.; Jeong, I.; Lee, J.; Lee, J.; Ko, M.J.; Lee, J.S. Unbiased Sunlight-Driven Artificial Photosynthesis of Carbon Monoxide from CO_2Using a ZnTe-Based Photocathode and a Perovskite Solar Cell in Tandem
ACS Nano **2016**, *10*, 6980.

[14] Chen, Y.; Li, C. W.; Kanan, M. W. Aqueous CO_2 Reduction at Very Low Overpotential on Oxide-Derived Au Nanoparticles
J. Am. Chem. Soc. **2012**, *134*, 19969.

[15] Ramdin, M.; de Loos, T. W.; Vlugt, T. J. H. State-of-the-Art of CO_2 Capture with Ionic Liquids
Ind. Eng. Chem. Res. **2012**, *51*, 8149.

[16] Rosen, B.A.; Salehi-Khojin, A.; Thorson, M. R.; Zhu, W.; Whipple, D. T.; Kenis, P. J. A.; Masel, R.I. Ionic Liquid–Mediated Selective Conversion of CO_2 to CO at Low Overpotentials
Science **2011**, *334*, 643.

[17] DiMeglio, J.L.; Rosenthal, J. Selective Conversion of CO_2 to CO with High Efficiency Using an Inexpensive Bismuth-Based Electrocatalyst
J. Am. Chem. Soc. **2013**, *135*, 8798.

[18] Li, C.W.; Kanan, M.W. CO_2 Reduction at Low Overpotential on Cu Electrodes Resulting from the Reduction of Thick Cu_2O Films
J. Am. Chem. Soc. **2012**, *134*, 7231.

[19] Kostecki, R.; Augustynski, J. Photon-Driven Reduction Reactions on Silver
J. Appl. Electrochem. **1993**, *23*, 567.
[20] Liu, S.; Tao, H.; Zeng, L.; Liu, Q.; Xu, Z.; Liu, Q.; Luo, J.-L. Shape-Dependent Electrocatalytic Reduction of CO_2 to CO on Triangular Silver Nanoplates
J. Am. Chem. Soc. **2017**, *139*, 2160.
[21] Zhang, L.; Wang, Z.; Mehio, N.; Jin, X.; Dai, S. Thickness-and Particle-Size-Dependent Electrochemical Reduction of Carbon Dioxide on Thin-Layer Porous Silver Electrodes
ChemSusChem **2016**, *9*, 428.
[22] Ma, M.; Trzesniewski, B.J.; Xie, J.; Smith, W.A. Selective and Efficient Reduction of Carbon Dioxide to Carbon Monoxide on Oxide-Derived Nanostructured Silver Electrocatalysts
Angew. Chem. Int. Ed. **2016**, *55*, 1.
[23] Kim, C.; Jeon, H.S.; Eom, T.; Jee, M.S.; Kim, H.; Friend, C.M.; Koun Min, B.; Hwang, Y.J. Achieving Selective and Efficient Electrocatalytic Activity for CO_2 Reduction Using Immobilized Silver Nanoparticles
J. Am. Chem. Soc. **2015**, *137*, 13844.
[24] Lu, Q.; Rosen, J.; Zhou, Y.; Hutchings, G.S.; Kimmel, Y.C.; Chen, J.G.; Jiao, F. A Selective and Efficient Electrocatalyst for Carbon Dioxide Reduction
Nat. Comm. **2014**, *5*, 3242.
[25] Zhang, Y.; Ji, L.; Qiu, W.; Shi, X.; Asiri, A. M.; Sun, X. Iodide-Derived Nanostructured Silver Promotes Selective and Efficient Carbon Dioxide Conversion into Carbon Monoxide
Chem. Commun. **2018**, *54*, 2666.
[26] Cho, M.; Seo, J.-W.; Song, J. T.; Lee, J.-Y.; Oh, J. Silver Nanowire/Carbon Sheet Composites for Electrochemical Syngas Generation with Tunable H_2/CO Ratios
ACS Omega **2017**, *2*, 3441.
[27] Qiu, W.; Liang, R.; Luo, Y.; Ciu, G.; Qiu, J.; Sun, X. A Br^- Anion Adsorbed Porous Ag Nanowire Film: in situ Electrochemical Preparation and Application Toward Efficient CO_2 Electroreduction to CO with High Selectivity
Inorg. Chem. Front. **2018**, *5*, 2238.
[28] Back, S.; Yeom, M. S.; Jung, Y. Active Sites of Au and Ag Nanoparticle Catalysts for CO_2 Electroreduction to CO
ACS Catal. **2015**, *5*, 5089.
[29] Daiyan, R.; Lu, X.; Ng, Y. H.; Amal, R. Highly Selective Conversion of CO_2 to CO Achieved by a Three-Dimensional Porous Silver Electrocatalyst
ChemistrySelect **2017**, *2*, 879.
[30] Ham, Y.S.; Choe, S.; Kim, M. J.; Lim, T.; Kim, S.-K.; Kim, J. Electrodeposited Ag Catalysts for the Electrochemical Reduction of CO_2 to CO
J. Appl. Catal. B: Environ. **2017**, *208*, 35.
[31] Fan, M.; Garbarino, S.; Botton, G. A.; Tavares, A.C.; Guay, D. Selective Electroreduction of CO_2 to Formate on 3D [100] Pb Dendrites with Nanometer-sized Needle-like Tips
J. Mater. Chem. A **2017**, *5*, 20747.

[32] Won, D.H.; Choi, C.H.; Chung, J.; Chung, M.W.; Kim, E.-H.; Woo, S.I. Rational Design of a Hierarchical Tin Dendrite Electrode for Efficient Electrochemical Reduction of CO_2
ChemSusChem **2015**, *8*, 3092.

[33] Medina-Ramos, J.; Pupillo, R. C.; Keane, T. P.; DiMeglio, J. L.; Rosenthal, J. Efficient Conversion of CO_2 to CO Using Tin and Other Inexpensive and Easily Prepared Post-Transition Metal Catalysts
J. Am. Chem. Soc. **2015**, *137*, 5021.

[34] Natter, H.; Hempelmann, R. Tailor-made Nanomaterials Designed by Electrochemical Methods
Electrochem. Acta **2003**, *49*, 51.

[35] Gurrappa, I.; Binder, L. Electrodeposition of Nanostructured Coatings and their Characterization - A Review
Sci. Technol. Adv. Mater. **2008**, *9*, 043001.

[36] Back, S.; Yeom, M. S.; Jung, Y. Active Sites of Au and Ag Nanoparticle Catalysts for CO_2 Electroreduction to CO
ACS Catal. **2015**, *5*, 5089.

[37] Hoshi, N.; Kato, M.; Hori, Y. Electrochemical Reduction of CO_2 on Single Crystal Electrodes of Silver Ag (111), Ag (100) and Ag (110)
J. Electroanal. Chem. **1997**, *400*, 283.

[38] Salomé, S.; Rego, R.; Oliveira, M.C. Development of Silver-gas Diffusion Electrodes for the Oxygen Reduction Reaction by Electrodeposition
Mater. Chem. Phys. **2013**, *143*, 109.

[39] Urbain, F.; Tang, P.; Carretero, N. M.; Andreu, T.; Gerling, L. G.; Voz, C.; Arbiol, J.; Morante, J.R. A Prototype Reactor for Highly Selective Solar-driven CO_2 Reduction to Synthesis Gas using Nanosized Earth-Abundant Catalysts and Silicon Photovoltaics

[40] Irtem, E.; Andreu, T.; Parra, A.; Hernández-Alonso, M. D.; García-Rodríguez, S.; Riesco-García, J. M.; Penelas-Pérez, G.; Morante, J.R. Low-energy Formate Production from CO_2 Electroreduction using Electrodeposited Tin on GDE
J. Mater. Chem. A **2016**, *4*, 13582.
Energy Environ. Sci. **2017**, *10*, 2256.

[41] Hernández-Alonso, M. D.; Penelas-Pérez, G.; Andreu, T.; Irtem, E.; Parra, A.; Fábrega, C.; Morante, J.R. Filter-press Photoelectrochemical Water Oxidation and CO_2 Reduction Cell, Patent WO/2016/097247, 23 June 2016.

[42] Min, S.; Yang, X.; Lu, A.-Y.; Tseng, C.-C.; Hedhili, M. N.; Li, L.-J.; Huang, K.-W. Low Overpotential and High Current CO_2 Reduction with Surface Reconstructed Cu Foam Electrodes
Nano Energy **2016**, *27*, 121.

[43] Yu, J.; Xiong, J.; Cheng, B.; Liu, S. Fabrication and Characterization of Ag–TiO_2 Multiphase Nanocomposite Thin Films with Enhanced Photocatalytic Activity
Appl. Catal. B: Environ. **2005**, *60*, 211.

[44] Stathatos, E.; Lianos, P.; Falaras, P.; Siokou, A. Photocatalytically Deposited Silver Nanoparticles on Mesoporous TiO_2 Films
Langmuir **2000**, *16*, 2398.
[45] Arbiol, J.; Fontcuberta i Morral, A.; Estradé, S.; Peiró, F.; Kalache, B.; Roca i Cabarrocas, P.; Morante, J.R. Influence of the (111) Twinning on the Formation of Diamond Cubic/Diamond Hexagonal Heterostructures in Cu-Catalyzed Si Nanowires
J. Appl. Phys. **2008**, *104*, 064312.
[46] Spirkoska, D.; Arbiol, J.; Gustafsson, A.; Conesa-Boj, S.; Glas, F.; Zardo, I.; Heigoldt, M.; Gass, M. H.; Bleloch, A. L.; Estrade, S.; Kaniber, M.; Rossler, J.; Peiro, F.; Morante, J.R.; Abstreiter, G.; Samuelson, L.; Fontcuberta i Morral, A. Structural and Optical Properties of High Quality Zinc-blende/Wurtzite GaAs Nanowire Heterostructures
Physical Review B **2009**, *80*, 245325.
[47] Utama, M. I. B.; de la Mata, M.; Magen, C.; Arbiol, J.; Xiong, Q. Twinning-, Polytypism-, and Polarity-Induced Morphological Modulation in Nonplanar Nanostructures with van der Waals Epitaxy
Adv. Func. Mater. **2013**, *23*, 1636.
[48] Ulissi, Z. W.; Tang, M. T.; Xiao, J.; Liu, X.; Torelli, D. A.; Karamad, M.; Cummins, K.; Hahn, C.; Lewis, N. S.; Jaramillo, T. F.; Chan, K.; Nørskov, J.K. Machine-Learning Methods Enable Exhaustive Searches for Active Bimetallic Facets and Reveal Active Site Motifs for CO_2 Reduction
ACS Catal. **2017**, *7*, 6600.
[49] Nesbitt, N-T.; Ma, M.; Trześniewski, B.J.; Jaszewski, S.; Tafti, F.F.; Burns, M.J.; Smith, W.A.; Naughton, M.J. Au Dendrite Electrocatalysts for CO_2 Electrolysis
J. Phys. Chem. C, **2018**, *122*, 10006.
[50] Whipple, D. T.; Finke, E. C.; Kenis, P.J.A. Microfluidic Reactor for the Electrochemical Reduction of Carbon Dioxide: the Effect of pH
Electrochem. Solid State Lett. **2010**, *13*, D109.
[51] Delacourt, C.; Ridgway, P. L.; Kerr, J. B.; Newman, J. Design of an Electrochemical Cell Making Syngas ($CO+ H_2$) from CO_2 and H_2O Reduction at Room Temperature
J. Electrochem. Soc. **2008**, *155*, B42.
[52] Salehi-Khojin, A.; Molly Jhong, H.-R.; Rosen, B. A.; Zhu, W.; Ma, S.; Kenis, P. J. A.; Masel, R.I. Nanoparticle Silver Catalysts that Show Enhanced Activity for Carbon Dioxide Electrolysis
J. Phys. Chem. C **2013**, *117*, 1627.
[53] Verma, S.; Lu, X.; Ma, S.; Maseld, R. I.; Kenis, P.J.A. The Effect of Electrolyte Composition on the Electroreduction of CO_2 to CO on AgBased Gas Diffusion Electrodes
Phys. Chem. Chem. Phys. **2016**, *18*, 7075-7084.
[54] Hernández, S.; Farkhondehfal, M.A.; Sastre, F.; Makkee, M.; Saraccob, G.; Russo, N. Syngas Production from Electrochemical Reduction of CO_2: Current Status and Prospective Implementation
Green Chem., **2017**, *19*, 2326-2346.

[55] Wang, Y.; Yuan, A.; Wang, X. Pseudocapacitive Behaviors of Nanostructured Manganese Dioxide/Carbon Nanotubes Composite Electrodes in Mild Aqueous Electrolytes: Effects of Electrolytes and Current Collectors
J Solid State Electrochem., **2008**, *12*, 1101–1107.
[56] Œuret, C.; Oliveira Vilar, E.; Bezerra Cavalcanti, E. Carbon Fibre Cloth as an Electrode Material: Electrical Conductivity and Mass Transfer
J. Appl. Electrochem., **2002**, *32*, 1175-1182.

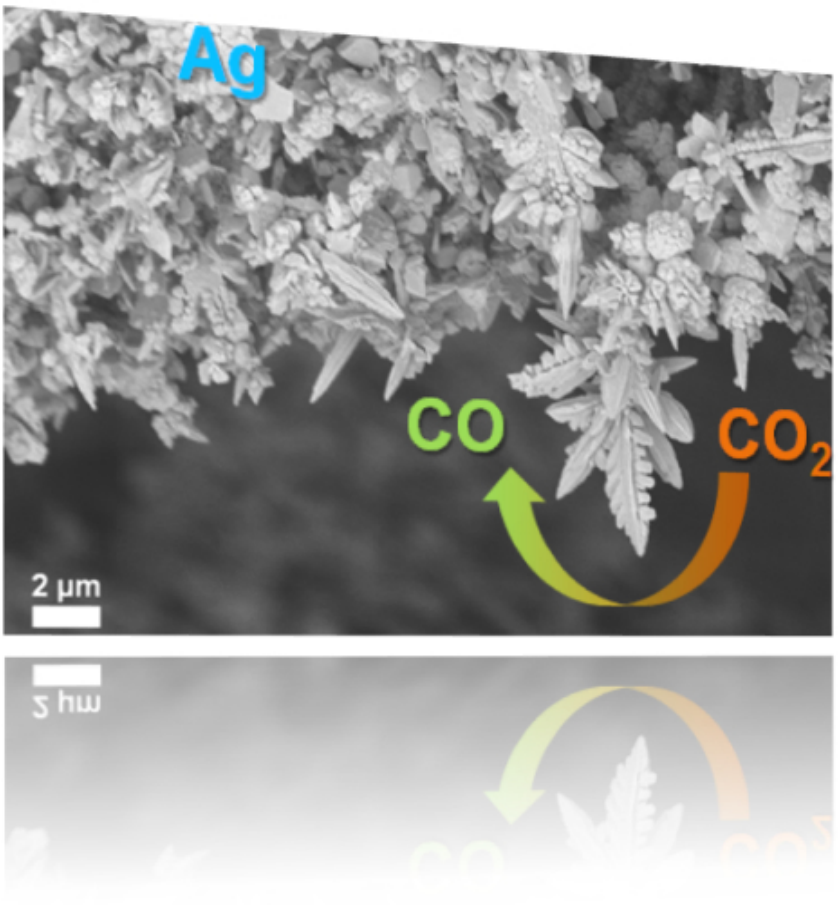
Ag
CO
CO_2
2 µm